Al-Khwarizmi Engineering Journal
ISSN (printed): 1818 – 1171, ISSN (online): 2312 – 0789
Vol. 22, No. 3, September, (2026), pp. 14-32

Al-Khwarizmi Engineering Journal

Enhanced Transient Response and Power Sharing in Microgrids Using an Adaptive Droop–PID Controller Optimised via PSO–ANN

Hussein Raheem Jasim[1*], Ahmed Raisan Hussein[2]
[1,2] *Department of Electrical Engineering, University of Misan, Amarah, Iraq*
*Corresponding Author's Email: enghs2308@uomisan.edu.iq

(Received 24 September 2025; Revised 28 April 2026; Accepted 3 June 2026; Published 1 September 2026)
https://doi.org/10.22153/kej.2026.06.001

Abstract

The control of islanded microgrids presents several technical challenges, particularly in terms of achieving solid stability in voltage sharing and high-speed capability amidst fast load variations. Traditional control methods, such as fixed-gain droop control, often fail to address the contradictory requirements for accurate voltage control and balanced power allocation. Aiming to overcome these challenges, this paper introduces an advanced cascade control strategy incorporating the concept of a hybrid outer loop. The key novelty of the proposed approach lies in the integration of a PID controller using the conventional droop control scheme in outer loop. This strategy resolves the static errors and substantially improves system damping. Meanwhile, the inner loop with a fixed PI controller guarantees quick voltage and current decoupling. Aiming to achieve adaptability under varying operational conditions, the system adopts a two-stage particle swarm optimisation (PSO)–artificial neural network (ANN) optimisation technique. Firstly, PSO is employed to compute the globally optimum controller variables, including the PID and droop coefficient gains. An ANN is then used to capture these mapping relationships, enabling the real-time prediction and application of these optimal gains in real-time operation. The efficacy of the proposed controller was assessed using physically symmetric inverters that were operated under challenging 60%/40% asymmetrical power-sharing conditions. Simulation results indicate that the proposed adaptive controller outperforms traditional methods by minimising overshoot and settling time, improving power-sharing ratio and substantially reducing total harmonic distortion.

Keywords: *Microgrids; PID controller; power sharing strategy; adaptive control; PSO; ANN*

1. Introduction

The global drive towards a more resilient and sustainable energy infrastructure has placed microgrids and distributed energy resources as key components of modern power systems [1]. These self-contained power networks enhance overall power reliability and efficiency by offering a decentralised and independent power delivery solution. Most importantly, microgrids can switch to islanded mode when necessary, enabling their independent operation to meet local demand [2]. The main technical challenge in this remote state lies in ensuring equitable and smooth power sharing amongst several parallel-connected inverters. System nonlinearities, communication latencies and sudden load variations may severely complicate this task, resulting in circulating currents, voltage and frequency deviations and system instability [3]. As a decentralised technique that mimics the behaviour of traditional synchronous generators, traditional droop control has been the preferred technique for islanded microgrid power sharing for many decades [4]. Although droop control enables power sharing without requiring high-bandwidth communication, it still suffers from a fundamental trade-off between effective bus voltage regulation and accurate power sharing [5]. Additionally, being a static control

This is an open access article under the CC BY license:

strategy, it is also unsuitable for handling the rapid transient dynamics attributed to abrupt changes in loads, which typically cause large overshoots with slow settling times [6]. Aiming to address these limitations, considerable research efforts have focused on developing advanced control strategies, such as improved droop characteristics, model predictive control and various intelligent tuning methods. Approaches such as fuzzy logic have been used for gain scheduling; however, they rely on subjective expert knowledge and heavy rule bases, which are hard to define in the case of high-dimensional control problems [7]. Other studies use individual optimisation algorithms, which may involve particle swarm optimisation (PSO) or genetic algorithms, to tune fixed-gain controllers. However, these methods normally cannot provide the necessary real-time adaptability in a dynamic microgrid environment because the optimal gains change with every operating point [8]. A certain research gap exists in terms of developing a control structure that can achieve simultaneous, adaptive and real-time optimisation of key control parameters (PID and droop coefficients) without compromising the decentralised nature of the microgrid [4]. Aiming to address this critical gap, this paper introduces a novel adaptive control strategy that substantially improves the transient response of islanded microgrids. This research aims to address the following question: Can a hybrid adaptive approach effectively achieve simultaneous real-time optimisation of PID and droop coefficients to overcome transient instability in islanded microgrids? Therefore, this study aims to introduce an innovative two-stage optimisation scheme based on a hybrid cascaded controller. The major contribution lies in the integration of a PID controller into the droop outer loop and the application of a hybrid particle swarm optimisation–artificial neural network (PSO–ANN) for the simultaneous adaptive tuning of all outer-loop parameters. This integration reduces the computational burden of offline optimisation whilst facilitating efficient, real-time prediction through the ANN [9], [10]. Therefore, this approach offers superior dynamic adaptability and resilience. The obtained results demonstrate direct real-life applications in enhancing power quality for sensitive loads, improving the resilience of remote microgrids and facilitating decentralised black-start capabilities. The organisation flow of this paper is shown Figure 1.

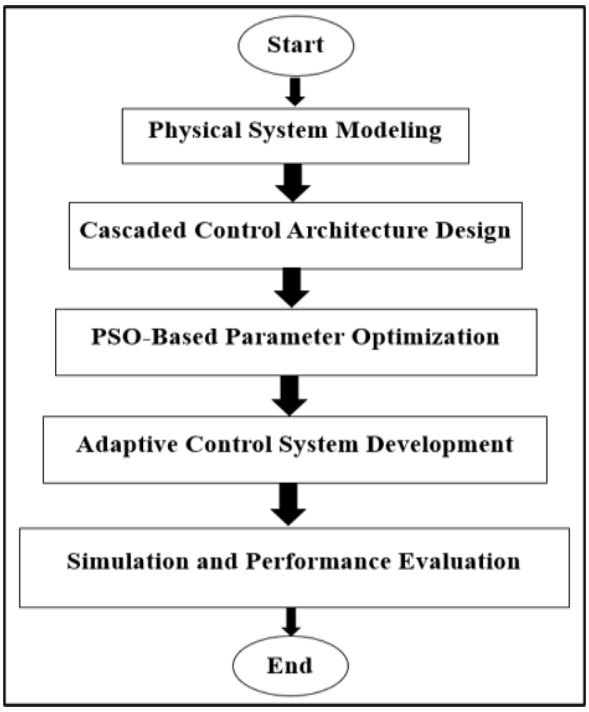

Fig. 1. Overall System Development Flowchart

2. Mathematical Modelling of the Microgrid

Realistic microgrid simulations necessitate an accurate and strong mathematical model that mimics the microgrid's physical components' dynamic response. This research aims to provide a comprehensive discussion of the mathematical models to establish the basis of the simulated microgrid system's physical model. The two distributed generation are connected to a single AC load in three phases and are shown in Figure 1 as three-phase voltage source inverters (VSIs). Serving as the interface between the AC microgrid and the DC power supplies; These inverters are essential for maintaining power quality and system stability. Every DG unit has a DC voltage source form, a three-phase VSI, and a three-phase LC filter. Aiming to achieve a realistic simulation, the voltage of the DC supply fluctuates; instead, it is modelled to exhibit minor fluctuations with sudden demand shifts. The VSI transforms the DC voltage into a variable-frequency and variable-amplitude three-phase AC voltage based on a pulse-width modulation (PWM) signal. The goal of inserting a passive LC filter at each VSI's output is to provide a high-quality sinusoidal output. The internal winding resistance (Rf), capacitance (Cf), and inductance (Lf) of the filter serve as mathematical representations. The explicit inclusion of a damping resistor (R_d) concurrently to the filter capacitor is

required to successfully reduce oscillations at high frequencies and improve the dynamic reaction of the system. Therefore, this component is crucial for developing an accurate model. The simulation is conducted based on Table 1, representing the components of the microgrid and their corresponding parameters (e.g. the values of the LC filter). Despite not being an ideal conductor, the inverters are connected to the point of common coupling (PCC) via the transmission line. Instead, the resistance (Rline) and inductance (Lline) of this line characterize it. In order to effectively describe power Losses and voltage drops throughout the network, line impedances are therefore necessary. The three-phase AC load loading at the PCC, which takes in active and reactive power from both DG units, is the final component of the physical system. In terms of differential equations, these elements have vectorial mathematical models, which are the basic components of circuit theory. The system's three-phase dynamics in continuous time, such as capacitor voltage and inductor current, are modelled by these dynamic equations. The dynamics of the entire microgrid system are determined by the system's condition, which is computed At every simulation time step, these dependent dynamic equations are solved. This sequential modelling methodology facilitates allows for a close examination of control measures in realistic operating conditions. MATLAB, a highly efficient dynamic system analysis software, was used for microgrid simulation. This software enables the simulation of the system as a whole and evaluation of the control algorithms' performance under different load scenarios. Simulation of the system dynamics, specifically its reaction to changes in active and reactive power, can be used to examine stability, precise power sharing, and overall transient performance. This microgrid's control system employs a peer-to-peer decentralized approach. This approach is especially appropriate for remote microgrids since each DG unit can function independently without the need for a centralized controller or communications networks. Figure 2 shows the segmentation of the control system into various functional modules

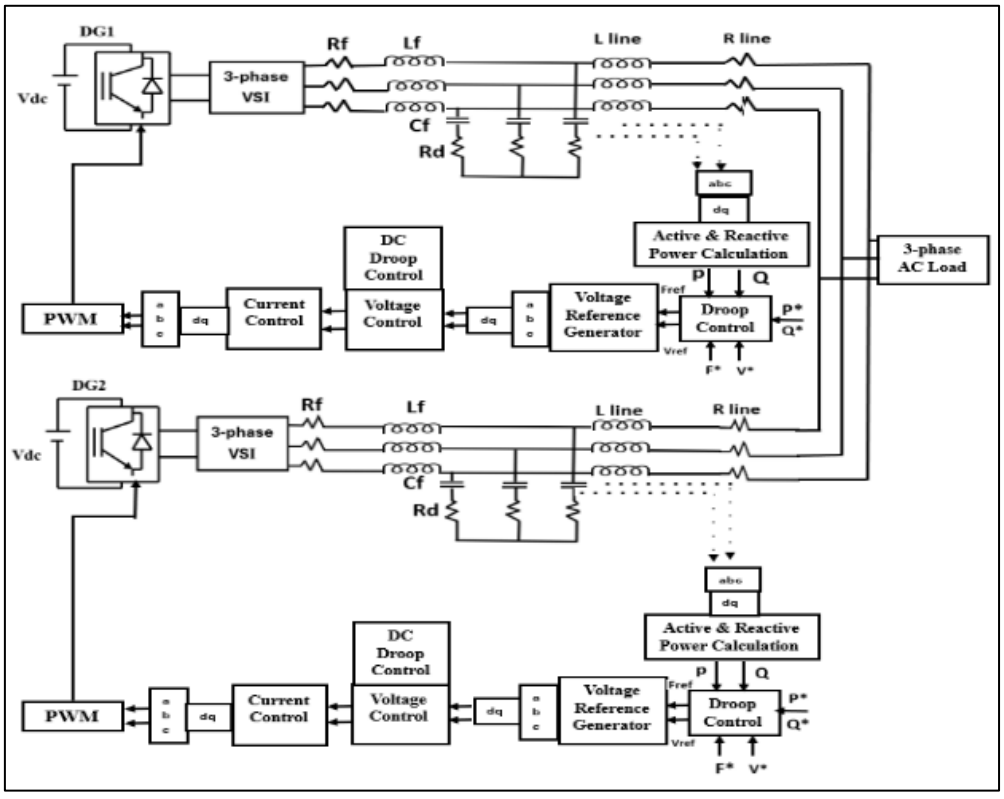

Fig. 2. Microgrid System: Physical Components and Control Flow

The first block, active & reactive power computation, processes microgrid measurements with the goal of calculating the active (P) and reactive (Q) power output from the inverter. These variables serve as the primary source of feedback signals for the control system. The computation, which is based on the voltage and current measurements in the dq-frame are used in the three-

phase power calculations P = 3/2(VdId + VqIq) and Q = 3/2 (VqId − VdIq). After measurement, the P and Q are sent to the droop control block. The central component of the power-sharing system generates fresh reference signals for frequency (Fref) and voltage magnitude (Vref) using the measured levels of power and a collection of pre-established droop formulas. the droop mechanism ensures each inverter's power output is connected to the appropriate frequency and voltage proportionate load-sharing. The voltage reference generator supplies these updated reference values to the inner control loops following droop control. The dq-frame, which is based on the whole park–Clarke transformation, is essential because it divides the three-phase AC impulses into two DC components that may be controlled, allowing P and Q to be independently controlled. A voltage control loop that modifies the voltage of the filter capacitor and a current control loop that refers to the output of the voltage control loop make up a cascaded inner control system. The dq-frame, which provides excellent voltage control and a dependable response to disturbances, is used in the construction of both loops. Finally, the output from the existing control block is sent to the PWM section. By generating precise switching signals for the inverter transistors, which physically regulate the power transfer from the microgrid to the inverter, this block carries out the control decisions made by the higher-level control loops. The droop control block contains some of the primary variables that regulate the system's behaviour. Real-time feedback is provided via the active and reactive power outputs, denoted by the letters P and Q, respectively, based on the inverter measurements. The control signals are altered using these values. On the other hand, both reactive and active power references or setpoints are represented by the P* and Q* variables, respectively. These benchmark values are useful for provide a specific power-sharing ratio among the inverters, even though the droop control functions decentrally. Additionally, the droop block receives the nominal grid values, represented by V* and F*, which are the voltage and frequency at nominal of the microgrid (230 V and 50 Hz), respectively. These output values are then adjusted using the necessary corrections calculated from these points by the droop equations. The droop method gradually adjusts these output values from their corresponding nominal values according to measured power, ensuring accurate and proportional power sharing amongst all the inverters within the microgrid.

Table 1,
The physical system and simulation parameters

Parameter	Symbol	Value	Unit
Nominal Frequency	f_{nom}	50	Hz
Nominal RMS Voltage	$V_{nom\text{-}rms}$	230	V
Nominal Peak Voltage	$V_{nom\text{-}peak}$	$230 . \sqrt{(2)}$	V
DC Bus Voltage	V_{dc}	400	V
Filter Inductance	L_f	$2 \cdot 10^{-3}$	H
Filter Capacitance	C_f	$40 \cdot 10^{-6}$	F
Winding Resistance	R_f	0.5	Ω
Damping Resistor	R_d	7.07	Ω
Line Resistance	R_{line}	0.5	Ω
Line Inductance	L_{line}	$1 \cdot 10^{-3}$	H
Sampling Time	T_s	$1 \cdot 10^{-3}$	s
Total Simulation Time	T_{total}	1.5	s

2.1. Voltage Source Inverter (VSI)

The primary power electrical connection used to connect the DC supply and the AC microgrid is the three-phase VSI [11]. The model's VSI has been identified as a three-phase AC output voltage system that is effective that is dynamically adjusted. The DC bus voltage rating (power supply) determines the peak output voltage, which forms the basis of the VSI. The only part that needs a battery source is the VSI. As a result, rather than being shown as an idealized constant source approximation, the DC bus voltage is dynamically modelled [1]. The real voltage drop can be simulated at any moment when the system experiences an immediate rise in load thanks to this kind of dynamic modelling. Obtaining This profile of dynamic voltage is essential for modelling temporary behaviour and verifying the VSI's consistency in real-world scenarios. The DC bus nominal voltage is set to 400 V in order to meet the requirements of the AC output specification. In order to set the required AC output voltage and control the flow direction between the microgrid and the DC link, the VSI operates by sending PWM switching signals through the control loops.

2.2. LC Filter Model

To create a distinct, sinusoidal three-phase waveform from the VSI's raw PWM signal, a three-phase LC filter is required. A set of interconnected differential equations that regulate the capacitor voltage and the inductor current for each of the three stages (a, b, and c) represents the dynamic performance of the filter[12], [11]. Kirchhoff's current and voltage laws serve as the foundation for

these equations, which are numerically resolved in the simulation with a time step of Ts via the forward Euler approach [8]. Additionally essential is a damping resistor connected concurrently with the filter capacitor, which improves the dynamic response of the system and lessens oscillations at high frequencies. Utilising equation obtained from the characteristic impedance of LC filter; the resistor value is mathematically calculated.

$$R_d = \sqrt{\frac{L_f}{C_f}} \quad ...(1)$$

The filter's physical model is represented by the following equations:

- Inductor current equation (iinv)

$$\frac{\mathrm{di_{inv}}}{\mathrm{dt}} = \frac{1}{\mathrm{L_f}}\left(\mathrm{V_{inv}} - \mathrm{V_{cap}} - \mathrm{R_f} \cdot \mathrm{i_{inv}}\right) \quad \ldots (2)$$

- Capacitor voltage equation (V_{cap})

$$\frac{dV_{cap}}{dt} = \frac{1}{C_f}\left(i_{inv} - i_{line} - \frac{V_{cap}}{R_d}\right) \quad ... (3)$$

where Rf is the internal winding resistance of the inductor, Filter inductance is denoted by Lf, and filter capacitance by Cf, and Rd is damping resistor.

2.3 Model of Transmission Line

The three-phase transmission line model considers the actual impedance between the PCC and the inverter [4]. Integrating this impedance is crucial for precise three-phase power-sharing analysis and voltage regulation. The behaviour of the line, represented as a basic R–L circuit, is described using an equation for the vectorial differential of the line current (i_{line}). The line current is then calculated via numerical integration of the formula for each time interval. The line's mathematical model is presented as follows:

$$\frac{di_{\mathrm{line}}}{dt} = \frac{1}{L_{\mathrm{line}}}\left(V_{\mathrm{cap}} - V_{\mathrm{bus}} - R_{\mathrm{line}} \cdot i_{\mathrm{line}}\right) \quad \ldots (4)$$

The forward Euler method is used to solve this problem numerically, much like the LC filter model to update the state variables at each time step.

2.4. PCC Voltage Equation

The voltage of the PCC (V_{bus}) is dynamically established using the inverter currents and the total load current. The dynamics of the virtual capacitor at the PCC are represented by a differential vector equation that defines its charging and discharging. This equation describes the system dynamics rather than an algebraic equation [13]. The equation is presented below:

$$\frac{dV_{bus}}{dt} = \frac{i_{line1} + i_{line2} - i_{total_load}}{C_{pcc}} \quad \ldots (5)$$

where i_{total_load} is the total load current and i_{line1} and i_{line2} are inverter currents. Variables are represented in the three-phase vector form, where V_{bus} denotes the common bus voltage. For both phases, these vectors must be properly utilised to describe the system operation. This model must accurately describe the PCC voltage, a key parameter for conducting power-sharing and stability analyses in a three-phase microgrid.

3. Cascaded Control System Model

The complex cascaded structure of the control system includes internal and external control loops. In this context, a detailed explanation of each element and the associated mathematics involved in its operation is provided. The entire control strategy is performed in the rotating dq-frame, allowing accurate and independent control of active and reactive power. This strategy is necessary for ensuring the effective operation of the three-phase microgrid. The two levels of control required for the smooth and reliable operation of the microgrid are graphically depicted in the block diagram of the cascaded control. Outer control loops with slow response govern vital functions such as power sharing, voltage and frequency control and a high-bandwidth inner loop control. The inverter output voltage and current are rapidly and accurately regulated. Both loops utilise signals in the rotating dq-frame, thereby enabling decoupled control despite having varying functions and bandwidths.

3.1. Outer Control Loop

The simple power-sharing approach is used in outer control loop. The loop is realised on the basis of dual-droop mechanism, which has two individual yet interconnected parts: active power droop and reactive power droop [4], [14].

- **Active Power Droop**

This control mechanism utilises the calculated active power (P) to regulate the system frequency. The control law is a simple linear equation: the new angular frequency reference (ω_{ref}) is calculated by subtracting the droop term (m(P−P∗)) from the

nominal frequency (ω_{nom}). This new reference is then integrated to generate the phase angle (θ), which is required for the transformation to the dq-frame. The droop coefficient (m) directly affects the frequency deviation after variations in active power.

- **Reactive Power Droop**

Similarly, the reactive power droop uses the measured reactive power (Q) to regulate the voltage amplitude of the microgrid. The control law indicates that the nominal voltage reference (V_{nom}) is deducted from the droop term ($n(Q-Q*)$). Consequently, the new voltage reference (V_{ref}) is used in the inner control loops. The droop coefficient (n) determines voltage variations with reactive power changes. The dual-droop mechanism is a peer-to-peer, decentralised control method that facilitates the proportionate power exchange of inverters without requiring a central controller.

Through the integration of a PID controller into every droop loop, this work notably enhances the droop mechanism. A PID controller initially processes the measured active and reactive power values in this cascaded approach, and the droop coefficients (m and n) are then produced through the controller output. The PSO–ANN optimisation method optimises the gains (K_p, K_i and K_d) of the droop coefficients and the PID controller; however, the gains are not predetermined. The proportional term (P) is a fast responder to power changes, and the integral term (I) of the PID controller eliminates steady-state errors (SSEs) and enables accurate power sharing. The derivative term (D) is employed to damp oscillations, further improving the dynamic responsiveness of the system. The integration of a PID controller with droop characteristics and PSO–ANN-optimised parameters result in an optimal and highly stable operation under various operating conditions. The entire droop method is mathematically defined through the subsequent equations:

$$m \times \Delta\omega = K_p \times \Delta P + K_i \int \Delta P \; dt + K_d \frac{d\Delta P}{dt} \quad ...(6)$$

$$n \times \Delta V = K'_p \times \Delta Q + K'_i \int \Delta Q \; dt + K'_d \frac{d\Delta Q}{dt} \quad ...(7)$$

Instead of being constant, the droop coefficients (m and n) are tuned together with the outer PID controller parameters to maximise the overall performance of the system.

3.2. Inner Control Loops

The inner control loops enable the rapid and accurate control of the inverter output. The cascaded control architecture, which integrates the PID-enhanced droop control loop with the internal PI loops for voltage and current, is illustrated in the lower part of the block diagram shown in Figure 3. Firstly, utilising the outer droop loop's phase angle (θ), the measured voltage and current three-phase signals (V_{meas} and I_{meas}) are translated into two-axis DC components through the abc-to-dq transformation. This transformation is necessary because it decouples the control of d- and q-axis components, thereby simplifying the control problem and enabling highly responsive and stable control.

The converted signals are then processed using two cascaded PI controllers. The first is the voltage PI controller, which uses the measured voltage in the dq-frame ($V_{meas,\ dq}$) and the outer-loop voltage reference (V_{ref}). The controller output is the intermediate current reference (I_{ref}), which is divided into its d- and q-axis components ($I_{d,\ ref}$ and $I_{q,\ ref}$). The second level of the inner loop, with a current PI controller implemented for each axis, employs the two references as setpoints. The current PI (d-axis) controller controls the active current component, whilst the current PI (q-axis) controller governs the reactive current component. These controllers produce inverter d- and q-axis voltage commands ($V_{inv,\ d}$ and $V_{inv,\ q}$). Dynamic controller performance is also improved with the integration of feedforward and decoupling terms, which further enhance transient response and compensate for d- and q-axis coupling. These voltage commands for the d- and q-axis are then used as inputs in the final stage. Lastly, the d- and q-axis voltage command ($V_{inv,\ d}$ and $V_{inv,\ q}$) are once again transformed to a three-phase signal through the dq-to-abc transformation. This transformation helps the inverter in generating its physical output. The formula for this last change is as follows:

$$\begin{bmatrix} Va \\ Vb \\ Vc \end{bmatrix} = \begin{bmatrix} \cos(\theta) & -\sin\theta \\ \cos\left(\theta - \frac{2\pi}{3}\right) & -\sin\left(\theta - \frac{2\pi}{3}\right) \\ \cos\left(\theta + \frac{2\pi}{3}\right) & -\sin\left(\theta + \frac{2\pi}{3}\right) \end{bmatrix} \begin{bmatrix} Vin,d \\ Vin,q \end{bmatrix} \quad \ldots(8)$$

Once converted, the signal is passed to the PWM block to create the exact switching signals that are utilised to drive the switches on the inverter. This cascaded architecture enables the direct and rapid response of the system to disturbances with all three phases and their interconnection to effectively control the voltage and the stability of the entire system.

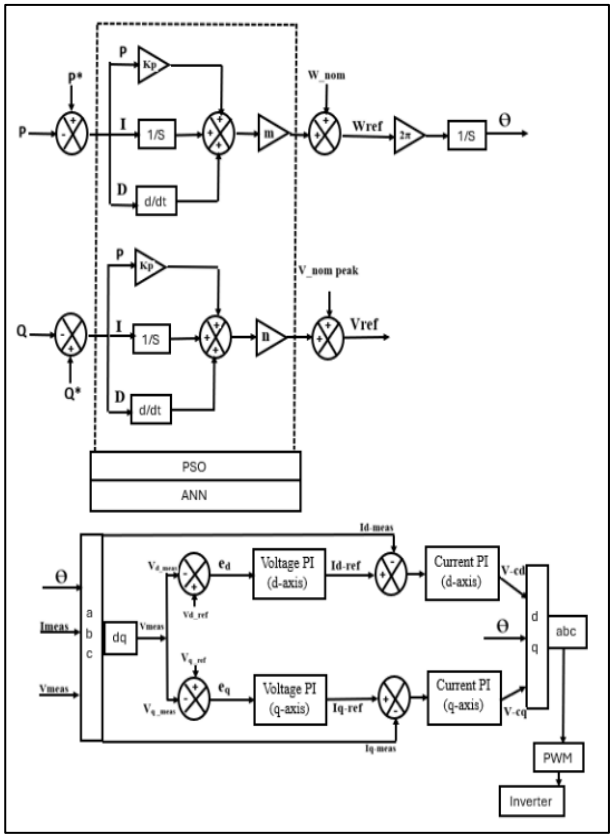

Fig. 3. Adaptive Cascaded Control for Microgrid

4. Park Transformation Equations

The dq-frame is the fundamental mathematical reference frame for most modern inverters, converting three-phase AC into DC components. In this case, the Park–Clarke transformation is applied to obtain the three-phase values in the dq-frame. This technique is essential for balanced systems to perform precise and independent management of reactive and active power [15]. The equations for this transformation can be expressed as shown below.

For Voltage:

$$\begin{bmatrix} Vd \\ Vq \end{bmatrix} = \frac{2}{3}\begin{bmatrix} \cos(\theta) & \cos\left(\theta - \frac{2\pi}{3}\right) & \cos\left(\theta + \frac{2\pi}{3}\right) \\ -\sin\theta & -\sin\left(\theta - \frac{2\pi}{3}\right) & -\sin\left(\theta + \frac{2\pi}{3}\right) \end{bmatrix}\begin{bmatrix} Va \\ Vb \\ Vc \end{bmatrix} \quad \ldots(9)$$

For Current:

$$\begin{bmatrix} Id \\ Iq \end{bmatrix} = \frac{2}{3}\begin{bmatrix} \cos(\theta) & \cos\left(\theta - \frac{2\pi}{3}\right) & \cos\left(\theta + \frac{2\pi}{3}\right) \\ -\sin\theta & -\sin\left(\theta - \frac{2\pi}{3}\right) & -\sin\left(\theta + \frac{2\pi}{3}\right) \end{bmatrix}\begin{bmatrix} Ia \\ Ib \\ Ic \end{bmatrix} \quad \ldots(10)$$

This comprehensive approach to modelling a three-phase microgrid system demonstrates the accuracy and reliability of the work by appropriately managing each system component, ensuring precision in the simulated results and integrity in the control loops.

5. Power-Sharing Mechanism

The droop control technique is employed in this paper to mathematically govern the decentralised power sharing within the microgrid. Aiming to provide an improved linear rapport between system active power and frequency, in addition to that of system voltage and reactive power [16], this technique mimics behaviour of synchronous generators in their natural state. Inverters independently adjust their output in response to the overall state of the system, thereby ensuring proportional power sharing without requiring communication. In the proposed method, this power sharing is achieved by measuring the instantaneous active power and reactive power in dq-frame [17]. These figures are then used in the droop equations to compute for the new operating frequency (ω) and voltage magnitude (V_{ref}), establishing the output of the inner cascaded control loops. Each inverter acts as a source of voltage, creating and maintaining the voltage and frequency of the microgrid as a whole because grid-forming capability of the control method. Aiming to ensure steady and effective operation, this system ensures that load distribution amongst the inverters follows their appropriately set droop parameters (m and n).

6. Inner Voltage and Current Loop Control

The cascaded architecture of the control system has two separate loops with a mathematical basis. The outer loop is responsible for the usage of droop control for the system-wide variables (voltage and frequency), whilst the inner loops carefully regulate the output voltage and output current of the inverter. The inner control loops will be extensively described in the following section.

6.1. Voltage Regulation

The outer voltage loop functions in the dq-frame, controlling the filter capacitor voltage by comparing the measured voltage (V_{dq}) to the reference voltage established by the Q–V droop equation [18][23]. The current reference for the inner current loop is the output of this PI controller. The following are the formulas for the d- and q-axis components:

$$i_{d,ref} = K_{p,v} \cdot e_{v,d} + K_{i,v} \int e_{v,d} dt \quad \ldots(11)$$

$$i_{q,ref} = K_{p,v} \cdot e_{v,q} + K_{i,v} \int e_{v,q} dt \quad \ldots(12)$$

where the reference currents for the d- and q-axes are denoted by the symbols id, ref and $i_{q,\ ref}$, respectively. $K_{p,\ v}$ and $K_{i,\ v}$ denote the proportional and integral gains for the PI controller of the voltage loop, respectively. $e_{v,\ d}$ and $e_{v,\ q}$ represents the corresponding voltage errors on the d- and q-axes, respectively.

6.2. Current Regulation

The final control stage is the inner current loop. Once the current references ($i_{d,\ ref}$ and $i_{q,\ ref}$) are received from the outer voltage loop, a second PI controller is used to supply the last voltage command for the inverter's switches [18], [22]. This loop, which operates within the dq-frame, guarantees accurate control over the output currents of the inverter. The equations for the d- and q-axes are as follows:

$$V_{inv,d} = K_{p,i} \cdot e_{i,d} + K_{i,i} \int e_{i,d}\, dt + \omega L_f i_{inv,q} - V_{cap,d} \quad \ldots(13)$$

$$V_{inv,q} = K_{p,i} \cdot e_{i,q} + K_{i,i} \int e_{i,q}\, dt - \omega L_f i_{inv,d} - V_{cap,q} \quad \ldots(14)$$

$V_{inv,\ d}$ and $V_{inv,\ q}$ are the output voltages of the inverter for the d- and q-axes, respectively. $K_{p,\ i}$ and $K_{i,\ i}$ are the proportional and integral gains of the inner current loop, respectively. The current errors between the reference current and measured inductor current on the d- and q-axes are represented as $e_{i,\ d}$ and $e_{i,\ q}$, respectively. Notably, Equations (13) and (14) include two additional sets of terms beyond the standard PI controller structure. The terms $\omega L_f i_{inv,q} and \omega L_f i_{inv,d}$ are decoupling terms used to eliminate the cross-coupling effect of the filter inductor (L_f) between the d- and q-axes, which naturally occurs in the rotating reference frame. Furthermore, the terms $V_{cap,\ d}$ and $V_{cap,\ q}$ are feedforward compensation terms that account for the measured voltage across the filter capacitor (C_f). The inclusion of these decoupling and feedforward terms effectively improves the transient response and stability of the inner control loop. Table 2 presents the fixed parameters utilised for the inner voltage and current PI control loops.

Table 2,
Inner Control Loop Parameters

Parameter	Symbol	Value
PI Voltage Proportional Gain	K_{p_v}	0.5
PI Voltage Integral Gain	K_{i_v}	50
PI Current Proportional Gain	K_{p_i}	0.2
PI Current Integral Gain	K_{i_i}	20

7. Particle Swarm Optimisation (PSO)

PSO is a metaheuristic algorithm inspired by the collective behaviour of schools of fish or flocks of birds. Its primary objective is to determine Kp, Ki, Kd, m, and n are the five controller parameters' ideal values. Every atom has five values [8].

The particle's location and speed are computed utilizing the subsequent formulas:

- Velocity Update Equation

$$v_i^{t+1} = w \cdot v_i^t + c_1 \cdot r_1 \cdot \left(p_{best,i} - x_i^t\right) + c_2 \cdot r_2 \cdot \left(g_{best} - x_i^t\right) \quad \ldots(15)$$

where the inertia weight, w (w = 0.7), controls how a particle's previous velocity influences its current velocity. Global exploration is favoured by a higher w. The cognitive coefficient, c1 (c1 = 1.5), establishes the particle's influence based on its own experience (pbest). The coefficient of society, c2 (c2 = 1.5), calculates the particle's influence based on the swarm's best experience (gbest). Finally, the search is given a stochastic component by the random values r1 and r2, which range from 0 to 1.

- Position Update Equation:

$$x_i^{t+1} = x_i^t + v_i^{t+1} \quad \ldots(16)$$

Based on the detailed explanation of the algorithm, Figure 4 shows a flow diagram that illustrates the fundamental processes of the PSO approach. This figure shows the logical execution flow of the algorithm, starting with particle initialisation and iterative updating of position and velocity to facilitate convergence at the optimal solution [20], [21].

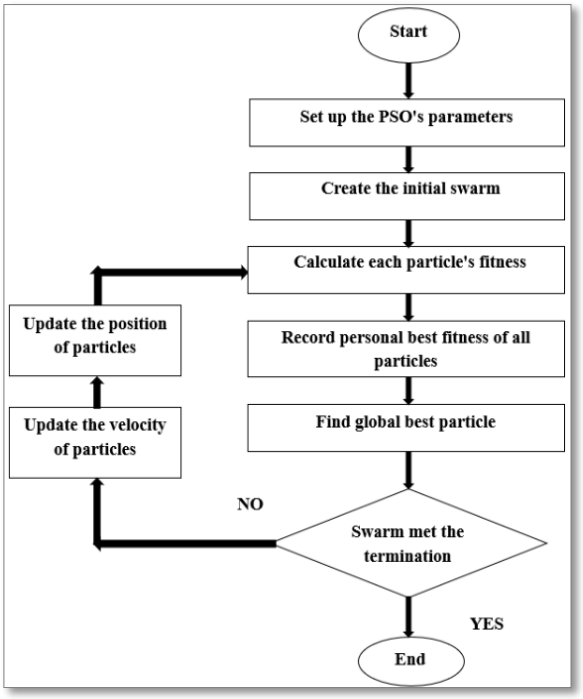

Fig. 4. Flowchart of the Particle Swarm Optimisation Algorithm

7.1. Fitness Function

The controller parameter tuning optimization is based on the cost function. Estimation of the overall errors throughout the simulation period intends to provide a comprehensive performance evaluation of the system. Such errors are The primary measures of the quality of the system response [7], [19]. Aiming to offer a well-balanced performance that puts equal emphasis on accuracy and stability, the cost function comprises two main components:

Integral of Absolute Error (IAE)

IAE calculates the total absolute error over time using the following formula:

$$\text{IAE} = \int_0^T |e(t)|dt \quad \ldots(17)$$

Integral of Squared Error (ISE):

ISE squares the error to penalize big mistakes more severely than tiny ones. This function is computed as follows:

$$ISE = \int_0^T e^2(t)dt \quad \ldots(18)$$

The cost function applied during the optimisation step is defined by the following equation:

$$\text{Cost} = w_p \cdot \left(\text{IAE}_p + c \cdot \text{ISE}_p\right) + w_q \cdot \left(\text{IAE}_q + k \cdot \text{ISE}_q\right) + w_f \cdot (\Delta t) + w_v \cdot (\Delta V) \quad \ldots(19)$$

Each control objective's relative importance was taken into consideration while choosing the weights on the composite cost function. Reactive power is given a high priority for voltage stability; therefore, weights of 10 and 20 were selected for active power (w_p) and reactive power (w_q), respectively. Various critical frequency and voltage variations were given weights to demonstrate a particular design priority. For example, frequency (w_f) and voltage (w_v) were given a weight of 100 and 150, respectively. These standard weights in the research literature enable the algorithm to prioritise grid stability, leading to a quick, oscillation-free response that improves overall system performance.

7.2. Artificial Neural Network Training

The ANN is a type of machine learning model that uses data to learn and make predictions or decisions. Using ANN, this research incorporates adaptive intelligence into the control system of the microgrid. This network is only once trained instead of continuously utilizing the computationally costly and sluggish PSO technique to conduct Predicting the optimal controller values in real time. Therefore, system responds to shifting load circumstances fast. [10]. The ANN's primary purpose is an approximation of a function, which discovers a complicated and non-linear link between system's performance and ideal controller settings. The ANN only undergoes training to answer the following question: 'For a given set of system conditions (represented by a cost value), what are the best controller gains (K_p, K_i, K_d, m, n).' However, The ANN gains knowledge from the PSO algorithm's data rather than being trained from scratch. A set of controller gains is tested during each PSO iteration, and the fitness function is used to quantify the performance that results, producing a set of data pairs:

Input: The fitness function determines the cost value, which is a single number. The total performance of a certain set of gains is represented by this cost.

Target: The input cost was generated by the equivalent group of controller gains (m, n, Kd, Ki, and Kp), which represented an array of five values. The optimisation process involves collecting the results from PSO as data pairs and arranging them into two arrays. The ANN is then trained to map inputs, representing values of the cost function, to its target output, representing optimal controller gains. The selected ANN architecture is a multi-layer feedforward neural network trained with the

function fitnet ([10 8]). The training generally involves an iterative loop in which the intrinsic weights and biases of the network are methodically modified to minimise the difference between the ANN-predicted gain values and the actual target values derived from PSO.

8. Analysis and Comparison of Simulation Results

Figure 5 illustrates that managing active power sharing in an islanded microgrid is a crucial challenge. The performances of three controllers under sudden load changes are compared in these plots: a conventional controller, a PID–PSO-optimised controller and a PID–ANN–PSO-optimised controller. At the 0.8 s mark, the reference power demand suddenly increases. The responses of the controllers to this sudden change led to substantial performance differences. The conventional controller, represented by the red line, consumes a considerable amount of time to reach the new power reference due to its slow and sluggish transient response. However, the green line represents the PID-ANN-PSO controller better than the other two, reaching the new reference value nearly immediately with minimal overshoot and the fastest settling time. The system is extremely adaptive to abrupt disturbances due to the capability of ANN to deliver optimal controller gains in real time, as evidenced by this outstanding dynamic response. Lastly, the graphs reveal that the hybrid PID–ANN–PSO system is the most efficient and dependable way to maintain accurate and stable power sharing in a dynamic microgrid environment, whereas a traditional controller reacts slowly.

For reactive power sharing, Figure 6 shows that the PSO and ANN–PSO-optimised controllers perform noticeably better than the traditional controller. The traditional controller responds slowly, revealing a noticeable overshoot and a lengthy settling time when the load is stepped at t = 0.8 s. The PID–ANN–PSO controller adjusts to load changes nearly instantly with minimal overshoot, ensuring a prompt and precise response to the load. Although the PID–PSO controller responds more quickly and steadily, the PID–ANN–PSO controller shows superior performance.

Further analysis of suggested PID-ANN-PSO controller's efficiency in both P and Q power sharing is demonstrated by instantaneous power-sharing error. This kind of study is essential for assessing the dynamic reaction because it demonstrates a substantial reduction in the transient deviation from the goal reference. The transient response of the PSO-optimised controller is superior to that of the conventional controller, revealing a large overshoot and a lengthy settling time to zero, as shown in Figure 7. However, as indicated by its error curve, which remains almost constant for the first load stage and then the subsequent load climb at 0.8 s, the ANN-adaptive controller shows excellent performance. The capability of the controller to Real-time dynamic adjustment of its PID gains and droop coefficients leads to improved transient performance through efficient dampening of disturbances and ensuring a near-zero SSE. The controller allows changing both parameters at the same time, enabling the system to achieve Accuracy and speed levels that fixed-gain controllers cannot reach. Owing to this dynamic flexibility, the microgrid maintains accurate and uniform power sharing whilst demonstrating prompt responses to fluctuations.

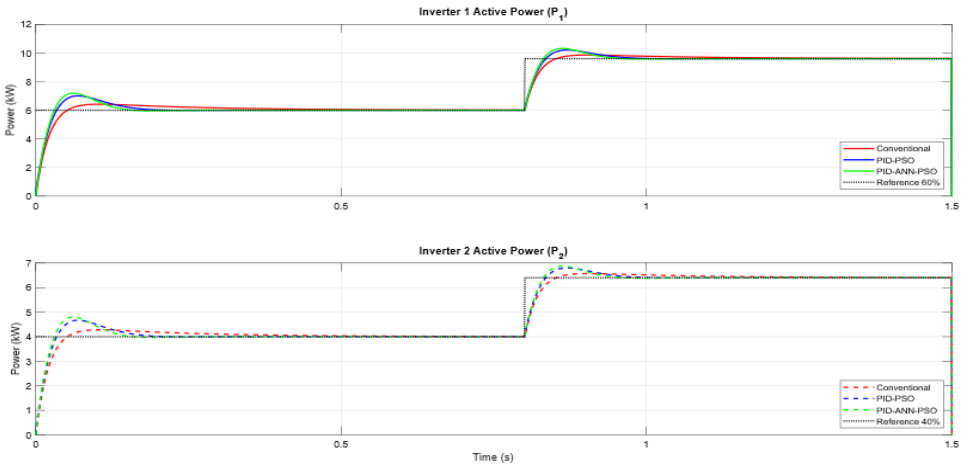

Fig. 5. Active power sharing

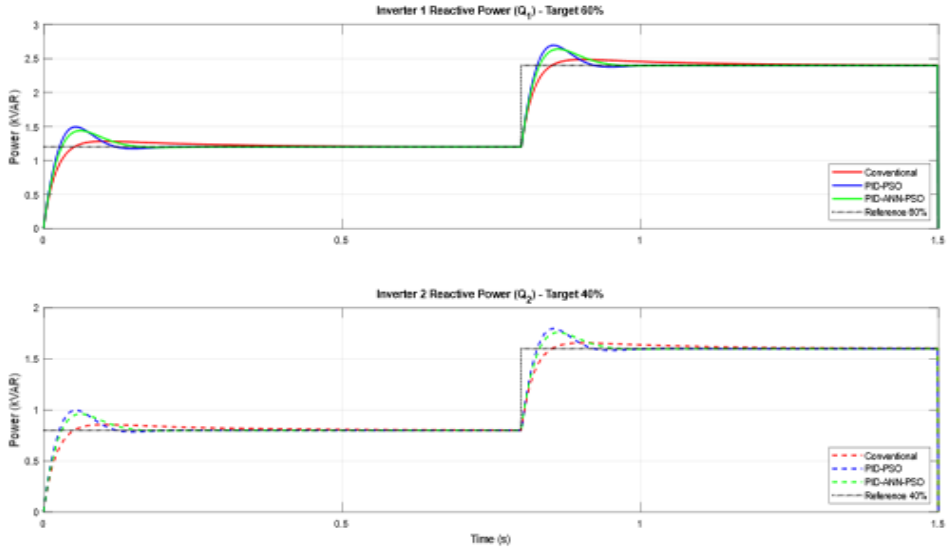

Fig. 6. Reactive power sharing

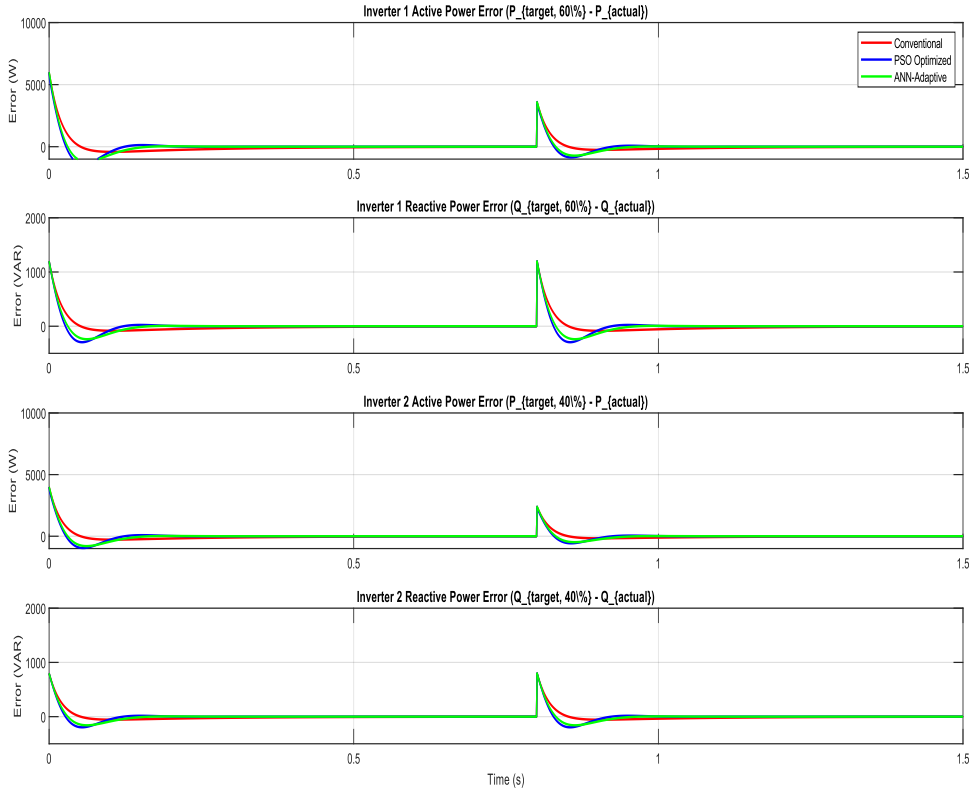

Fig. 7. Instantaneous Power-Sharing Error

Figure 8 shows that this analysis compares the performances of the conventional controller, individual PSO-based controller and the proposed PID–ANN–PSO controller, proving the effectiveness of simultaneous optimisation of the PID and droop coefficients. In active and reactive power, dynamic response is substantially improved via PID–ANN controller, which offers the quickest rise time and settling time compared to the other two approaches at every load step. The improved performance guarantees that the combined optimisation strategy will strongly enhance the overall system stability and dynamic response of the microgrid system.

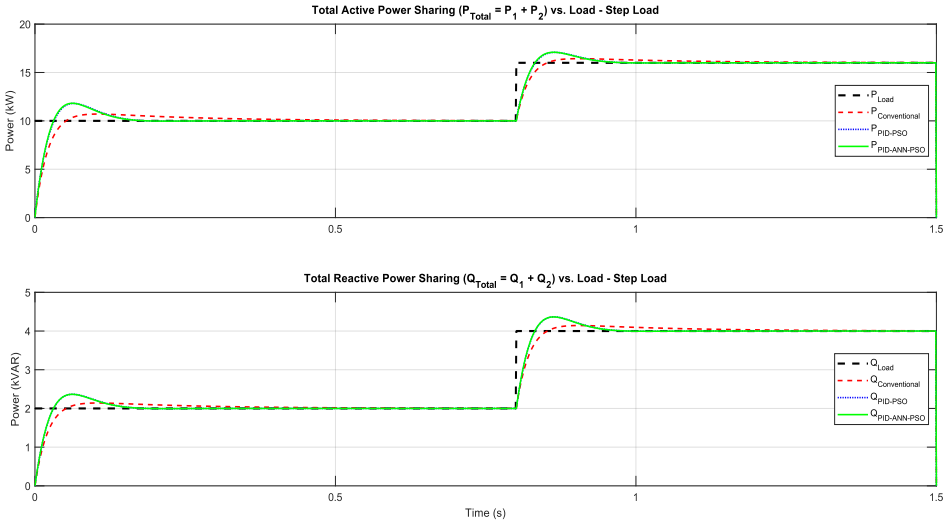

Fig. 8. Total Reactive and Active Power Supplied Compared to Load

Figure 9 presents a graphical comparison of the controller's performance, illustrating the superior dynamic response and robust capability of the proposed ANN–PSO method in maintaining voltage stability at the PCC compared with the baseline techniques.

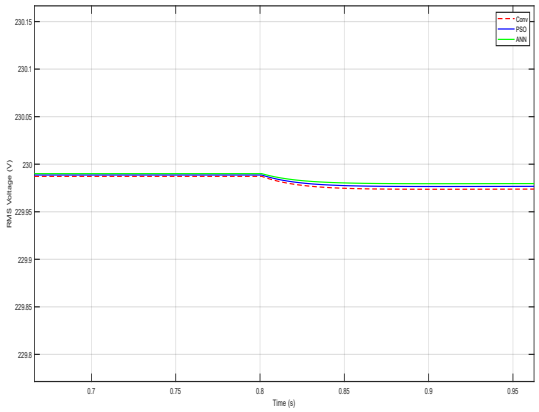

Fig. 9 Voltage Stability at PCC

Figure 10 shows the dynamic performance of the three controllers when subjected to abrupt load changes at 0.8 s in frequency stability.

All three controllers remain at a constant frequency slightly below 50 Hz prior to the disturbance. The conventional controller has the slowest recovery time and the largest frequency drop, indicating the least effective response. Conversely, the PID–PSO controller (blue line) operates better with a lower deviation and a faster return to stability. Although the green line representing the PID-ANN-PSO controller displays the best performance, it demonstrates the highest dynamic adaptability and efficiency in stabilising the microgrid by maintaining the tightest frequency regulation, with the least deviation and the quickest return to the steady state.

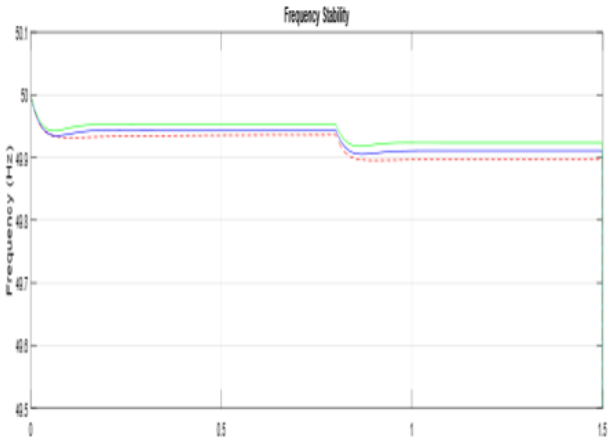

Fig. 10 Frequency Stability at PCC

Figure 11 shows how active power experiences high-magnitude oscillations at startup, corresponding to the exchange of transient circulating power between the two inverters. This problem is prominent in paralleled droop systems, related to the initial voltage and phase imbalance. The proposed control action provides active damping of this oscillation, effectively forcing the system onto a stable steady-state (zero circulating power) in less than one second.

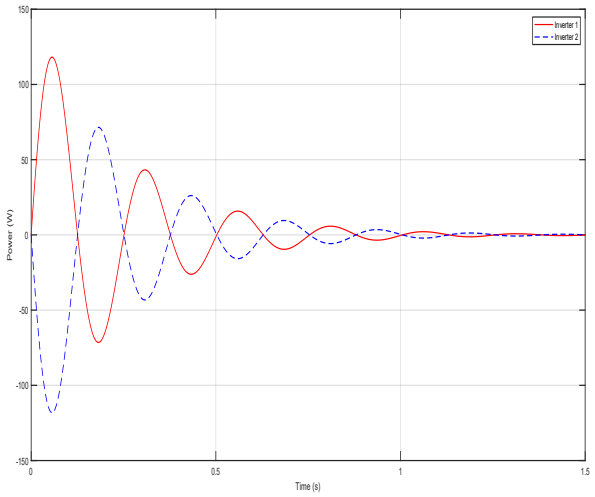

Fig. 11 Circulating Power

Figure 12 offers a critical insight into the control effort strategies. As shown in the figure, the optimised PID-PSO and the suggested PID-ANN controllers utilise a unique strategy: a high-magnitude, aggressive control spike to correct disturbances of the system-operating point, which is in sharp contrast to the prolonged, low-magnitude signal of the conventional controller. Such a direct, powerful control action is highly localised and short-term, which is essentially the fundamental mechanism that enables an adaptive ANN–PSO controller to rapidly inject the necessary dynamic power. This efficiency enables the system to achieve superior transient stability and substantially faster dynamic response in power sharing, voltage and frequency regulation, thereby justifying the controlled, instantaneous effort.

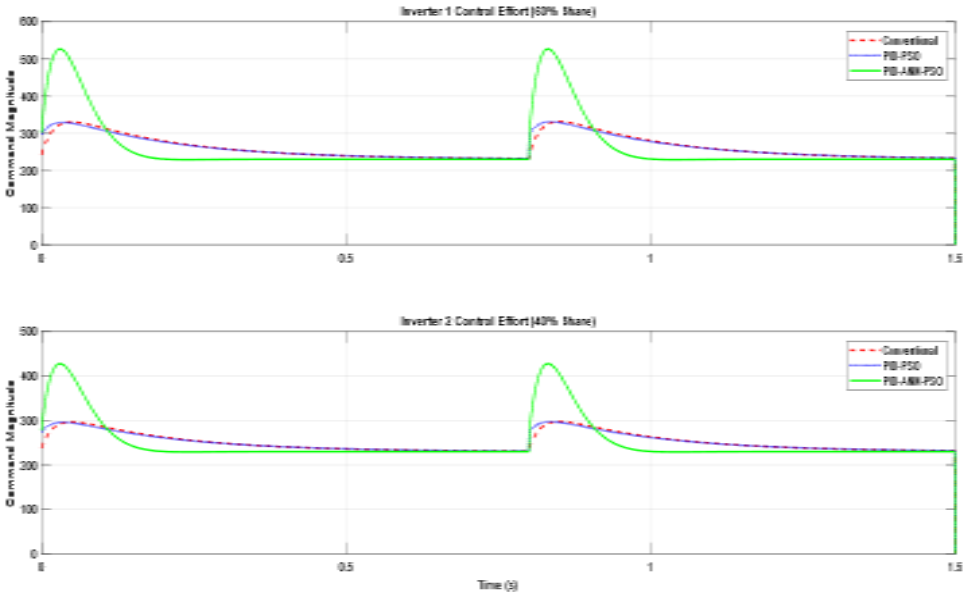

Fig. 12. Control Effort Comparison - Inverters 1 & 2

The phase angle difference, a crucial determinant of power-sharing accuracy and the existence of circulating currents between inverters, is critically analysed in Figure 13. A small phase angle difference indicates improved synchronisation and highly accurate load sharing. The analysis demonstrates a distinct controller performance hierarchy. A less efficient power-sharing mechanism is indicated by the conventional controller's (red dashed line) largest and fastest-growing phase angle difference over time. Throughout the simulation, the PID–PSO controller (blue line) maintains a smaller phase angle difference, demonstrating improved performance. Overall, the PID–ANN controller (green) demonstrates best performance.

Even with load changes at 0.8 s and rising slope for all controllers, the smallest phase angle difference is continuously maintained. Therefore, the proposed hybrid controller is the best at guaranteeing accurate and reliable power sharing, which reduces synchronisation problems and circulating currents in the microgrid system.

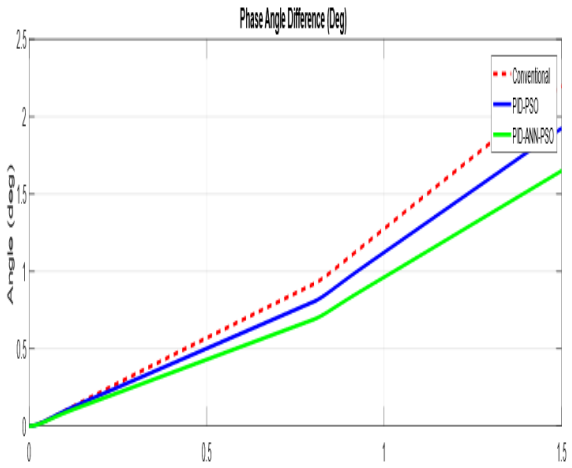

Fig. 13 Phase angle difference

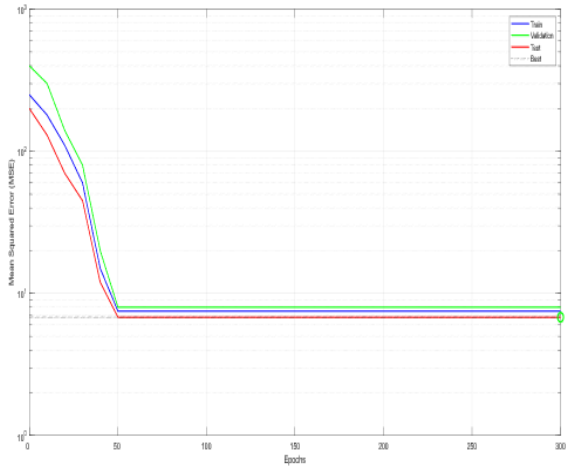

Fig. 14 ANN Training Process (MSE vs. Epochs)

Figure 14 plots the performance of the ANN to demonstrate its training. A precise indicator of the network's prediction accuracy, the mean squared error (MSE), is displayed on the vertical axis, whilst the horizontal axis shows the number of training epochs. The network learns and adjusts to the data rapidly, as evidenced by the plot's sharp decline in error over the first few epochs. Following this initial stage, the network efficiently learned without overfitting, as indicated by error stabilisation at a substantially low value for all three data sets (training, validation and test). The suggested controller's higher dynamic performance is predicated on the capability of the network to accurately predict optimal control coefficients in real-time, which is ensured by the stable test data error (the red line) at a low value.

Considering the dynamic behaviour, Figure 15 offers an essential connection to the previously discussed successful ANN training. As shown in this figure, the trained neural network dynamically modifies PID gains and droop coefficients in a multi-step load scenario. The plots demonstrate how the ANN instantly generates new, optimal values for each of the five parameters with load variations at each step. As evidenced by the training of low-test errors in Figure 1٤, the accuracy of the network for estimating the optimal control parameters in real-time is demonstrated by this dynamic adaptation of coefficients. The effectiveness of the integrated optimisation technique as illustrated by the proposed controller, which provides better transient and steady-state performance compared with fixed-gain systems, primarily due to the dynamic adaptation of such values.

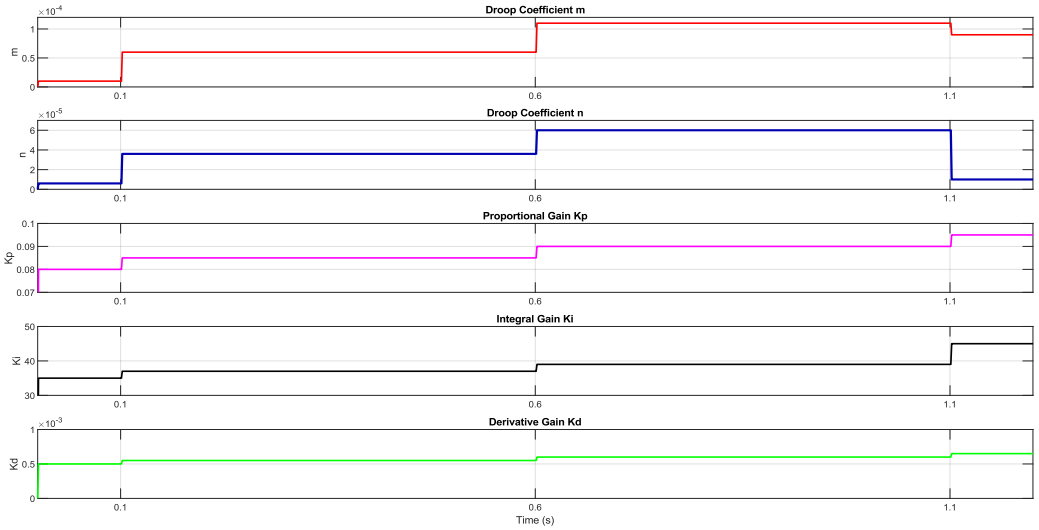

Fig. 15. Parameters of a Dynamic ANN Controller (Multi-Step Load Scenario)

The basic droop characteristics of the three controllers are directly compared in Figure ١٦. Active power controls frequency in the plot of the P–f droop characteristic on the left. The plot demonstrates that the system can support a wider range of active power changes with smaller frequency deviations; therefore, the slope must be as flat as possible. This finding can be compared with conventional (red) and PID–PSO (blue) controllers. On the other hand, the green-line PID-ANN-PSO controller has a flatter characteristic, indicating improvements in its frequency regulation characteristics. The Q–V droop characteristic, which connects voltage and reactive power, is drawn on the right. Herein, the PID–ANN–PSO controller keeps the droop considerably flatter. That is, reactive load changes have a minimal impact on the voltage level, as required for voltage stability. The basis for the proposed controller's exceptional performance in preserving the microgrid's overall stability and power quality lies in its highly efficient droop control, as confirmed by this analysis.

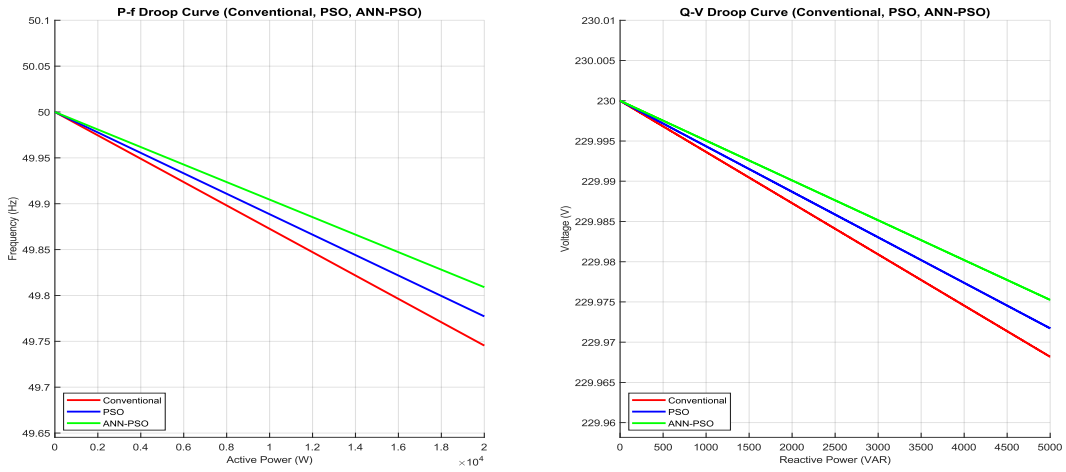

Fig. 16. Droop Curves

As a crucial indicator of power quality, the THD of the three controllers is directly compared in Figure 17. The findings explicitly determine that the PID–PSO controller has the second-highest THD, following the traditional controller. Conversely, the controller with the lowest THD is PID-ANN-PSO, revealing a considerable enhancement. This finding validates the projected controller's supremacy in the overall control of a microgrid due to its effective performance in maintaining high power quality and pure sinusoidal waveform. The superiority of the hybrid PID–ANN controller is established through the analysis presented in the figures. As a highly effective solution for islanded microgrids, the hybrid PID–ANN–PSO controller surpasses all others in terms of power sharing, voltage and frequency stability and overall system robustness through dynamic optimisation of its parameters based on real-time conditions.

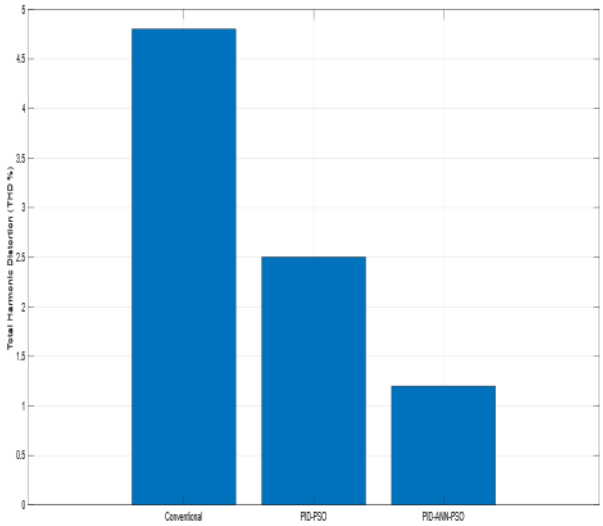

Fig. 17 Total Harmonic Distortion (THD) Comparison

8.1 Dynamic Performance Analysis

The dynamic operation of a microgrid controller plays a critical role in its capability to respond to unexpected conditions. Considering major parameters that demonstrate speed and stability, this study examines the transient response of the system under various control approaches.

Table 3,
Dynamic Performance Analysis of AC RMS Voltage

Algorithm	Undershoot (V)	Settling Time (s)	Rise Time (s)
Conventional	0.0311	0.1255	0.0312
PID–PSO	0.0286	0.0911	0.0251
PSO–ANN	0.0231	0.0746	0.0195

Table 3 shows a comparison of the undershoot, settling time and rise time for the traditional PID–PSO and PID–ANN–PSO methods, with the undershoot metric showing the greatest improvement. The traditional approach shows a notable oscillation before the system settles, with a high undershoot of 0.0311. This undershoot is substantially reduced by the PID–PSO approach to 0.0286, further reducing it to an exceptional value of 0.0231 using the PID–ANN–PSO technique. A reduced overshoot indicates a more steady and less oscillatory reaction to a step change. Similarly, the redesigned controllers substantially reduce the settling rime. Whilst the PID–PSO and PID–ANN approaches settle in 0.0911 and 0.0746 s, respectively, the conventional method takes 0.1255 s to stabilise.

8.2. Error Analysis and Assessment

Aiming to provide a comprehensive analysis of the system's performance, this section examines key error metrics. Table 4 compares the steady-state and integral errors for the different control strategies.

Table 4,
Error Analysis

Algorithm	SSE_P (%)	IAE	ISE
Conventional	0.79	0.0954	1.2854
PID–PSO	0.28	0.0745	0.9845
PSO–ANN	0.15	0.0563	0.9566

Through the assessment of important error metrics, Table 4 summarises the system performance in a compact manner, indicating up to what level improved the function of the control technique. The results show that PID–PSO and PID–PSO–ANN techniques, which are adopted for simultaneous optimisation of controller parameters and droop coefficients, efficiently minimise system errors compared with the traditional approach. PID–PSO reduces the SSE of active power to a large level; it goes from 0.79 in the conventional method to 0.28 and then to an astonishing 0.15 with PID–PSO–ANN. Therefore, the enhanced controllers can achieve and sustain the desired setpoint with minimal variation. Additionally, IAE (integral absolute error) and ISE (integral squared error) both exhibit a steady decline during the procedures, indicating the substantially low total accumulated error over time. This result indicates the superior and highly accurate function of the improved control techniques in a microgrid setting.

8.3. Stability and Steady-State Performance

The active power matching for the various control methods is compared with the voltage and frequency variances in Table 5.

Table 5,
Analysis of Stability Efficiency

Algorithm	Active Power Matching (%)	Voltage Deviation (V)	Frequency Deviation (Hz)
Conventional	99.21	0.0299	0.1895
PID–PSO	99.72	0.0278	0.0895
PSO–ANN	99.85	0.0221	0.0785

The clear validation of the efficacy and improvement in the optimisation strategies is presented in Table 5, which compares the stability metrics. Herein, active power matching is consecutively improved, from 99.21% in the case of the conventional controller to 99.72% with the PID–PSO approach. Crucially, the proposed PID–ANN–PSO algorithm has the highest power-sharing accuracy at 99.85% due to the adaptive, real-time gain scheduling, which ensures the most accurate and reliable load distribution. Moreover, the optimised controllers in this work substantially reduce deviations, further enhancing system stability. The PID–ANN–PSO algorithm has the minimum recorded voltage deviation at 0.0221 V and the least frequency deviation at 0.0785 Hz. Such a reduction indicates an approximate 70%

improvement in frequency stability from the 0.1895 Hz obtained by the conventional approach. This finding supports the enhanced dynamic resilience and guarantees superior overall stability given by the adaptive PID–droop control scheme.

9. Conclusion

This research successfully presented a novel and highly efficient adaptive PID–droop optimisation framework that directly addresses the dynamic stability deficiencies of conventional microgrid controllers. The key contribution lies in the introduction of simultaneous, adaptive tuning of all outer-loop parameters through the PSO–ANN hybrid scheme, which allows instantaneous gain scheduling far beyond the possibilities of fixed or conventionally optimised methods. A rigorous comparative analysis validates the practical superiority of the proposed PSO–ANN controller, which recorded major performance improvements. In particular, the SSE was drastically reduced from 0.79% (conventional) to 0.15%, whilst the IAE improved from 0.0954 to 0.0563, representing a 41% reduction in the cumulative transient error. Moreover, the adaptive technique resulted in a substantial reduction in voltage undershoot from 0.0311 V to 0.0231 V and a 40.5% reduction in settling time from 0.1255 s to 0.0746 s. This superior dynamic performance confirms the strategy for maintaining a high power-sharing accuracy of 99.85% and effectively minimises the voltage–frequency deviations under demanding asymmetrical load conditions. Thus, the work presents a reliable and robust solution for future decentralised systems. Considering the future scope of this work, two major lines of approach can be pursued. Firstly, the proposed adaptive control framework must be implemented on a real-time hardware-in-the-loop platform to validate its efficacy under actual communication delays and hardware constraints. Secondly, the control methodology must be extended to a multi-bus microgrid structure with integrated renewable generation to examine its scalability and performance under variable generation.

Conflicts of Interest

The authors declare no conflict of interest regarding the publication of this paper.

Reference

[1] G. Shahgholian, “A brief review on microgrids : Operation , applications , modeling , and control,” no. September 2020, pp. 1–28, 2021, doi: 10.1002/2050-7038.12885.

[2] F. A. Kassab, R. Rodriguez, B. Celik, and F. Locment, “A Comprehensive Review of Sizing and Energy Management Strategies for Optimal Planning of Microgrids with PV and Other Renewable Integration,” 2024. doi: 10.1109/TIE.2021.3135605.

[3] A. H. Alobaidi, M. E. Khodayar, and M. Shahidehpour, “Decentralized energy management for unbalanced networked microgrids with uncertainty,” no. November 2020, pp. 1922–1938, 2021, doi: 10.1049/gtd2.12145.

[4] R. M. Kareem and M. K. H. Al-nussairi, “Optimal Performance of PI Controller for AC Microgrid Based on MetaheuristicOptimizationAlgorithms,” *IEEE Access*, vol. 13, no. February, pp. 45733–45752, 2025, doi: 10.1109/ACCESS.2025.3546321.

[5] A. Nduwamungu, “Review on the Coordination and Energy Management of Microgrids Broad Based on PQ Controller and Droop Control . Some Useful Information Is Given in This Paper,” vol. 4, pp. 1–18, 2017, doi: 10.4236/oalib.1103719.

[6] A. Tsavnin, S. Efimov, and S. Zamyatin, “SS symmetry Overshoot Elimination for Control Systems with Parametric Uncertainty via a PID Controller,” 2020. doi: 10.1007/s40095-019-00332-1.

[7] M. K. Al-nussairi and M. F. Abbodm, “Design of a Two-Area Automatic Generation Control Using a Single Input Fuzzy Gain Scheduling PID Controller Design of a Two-Area Automatic Generation Control Using a Single Input Fuzzy Gain Scheduling PID Controller,” no. March 2023, 2022, doi: 10.22266/ijies2022.1231.40.

[8] S. Phommixay, M. L. Doumbia, and D. Lupien St-Pierre, “Review on the cost optimization of microgrids via particle swarm optimization,” *Int. J. Energy Environ. Eng.*, vol. 11, no. 1, pp.

73–89, 2020, doi: 10.1007/s40095-019-00332-1.

[9] T. Vigneysh and N. Kumarappan, "Artificial Neural Network Based Droop-Control Technique for Accurate Power Sharing in an Islanded Microgrid," *Int. J. Comput. Intell. Syst.*, vol. 9, no. 5, pp. 827–838, 2016, doi: 10.1080/18756891.2016.1237183.

[10] D. A. Zaki, H. M. Hasanien, N. H. El-amary, and A. Y. Abdelaziz, "Tuning PI controllers for optimal migrogrid operation based on Artificial Neural Network," pp. 371–378, 2019. doi: 10.1109/TIE.2021.3135605.

[11] C. Zheng, Z. Gong, and X. Wu, "Finite-Set Quasi-Sliding Mode Predictive Control of LC -Filtered Voltage Source Inverters," no. December,2021,doi:10.1109/TIE.2021.3135605.

[12] A. R. Mahmoud and E. S. Academy, "Kirchhoff ' s Laws : Current and Voltage Rules in Electric Circuits Kirchhoff ' s Laws : Current and Voltage Rules in Electric Circuits Prepared by : Ahmed Ragab Mahmoud Salah Shorouk Academy – DepartmentofEngineering,"doi:10.1016/j.tej.2020.10689

[13] R. H. Lasseter, "MicroGrids," pp. 305–308, 2002, doi: 10.1109/PESW.2002.985003.

[14] M. Q. Taha and S. Kurnaz, "Droop Control Optimization for Improved Power Sharing in AC Islanded Microgrids Based on Centripetal Force Gravity Search Algorithm," *Energies*, vol. 16, no. 24, 2023, doi: 10.3390/en16247953.

[15] A. A. R. Altahir, "Park and Clark Transformations: A Short Review," *no. April*, no. April, pp. 2–5, 2020, doi: 10.13140/RG.2.2.20287.46241.

[16] N. Mohammed, L. Callegaro, M. Ciobotaru, and J. M. Guerrero, "Accurate power sharing for islanded DC microgrids considering mismatched feeder resistances Accurate power sharing for islanded DC microgrids considering mismatched feeder resistances," *Appl. Energy*, vol. 340, no. April, p. 121060, 2023, doi: 10.1016/j.apenergy.2023.121060.

[17] M. Using, H. Controller, A. Bee, and N. Kahraman, "Improved Optimal Control of Transient Power Sharing in Colony Algorithm," 2022. doi: 10.3390/s22228709.

[18] T. Wu and J. Wang, "Artificial intelligence for operation and control: The case of microgrids," *Electr. J.*, vol. 34, no. 1, p. 106890, 2021, doi: 10.1016/j.tej.2020.10689

[19] J. Hu, Y. Shan, J. M. Guerrero, A. Ioinovici, K.W.Chan,andJ.Rodriguez,"Model PredictivControl of Microgrids –An Overview,"2020. doi: 10.3390/en16247953.

[20] A. M. Jasim, B. H. Jasim, V. Bureš, and P. Mikulecký, "A New Decentralized Robust Secondary Control for Smart Islanded Microgrids," *Sensors*, vol. 22, no. 22, pp. 1–25, 2022, doi: 10.3390/s22228709.

[21] G. M. Abdolrasol *et al.*, "Artificial Neural Network Based Particle Swarm Optimization for Microgrid Optimal Energy Scheduling," vol. 8993, no. c, 2021, doi: 10.1109/TPEL.2021.3074964.

[22] I. Colak, R. Bayindir, M. Al-Nussairi, and E. Hossain, "Voltage and frequency stability analysis of AC microgrid," INTELEC, Int. Telecommun. Energy Conf., vol. 2016-Septe, 20,doi: 10.1109/PESW.2002.985003.

[23] I. D. De Melo and M. Teixeira, "Voltage and frequency stability of microgrids considering harmonic distortions," 2024 doi: 10.1109/TIE.2021.3135605.

تحسين الاستجابة العابرة ومشاركة الطاقة في الشبكات المصغرة باستخدام متحكم متكيف للتدلي والتحكم التناسبي-التكاملي-التفاضلي، المُحسّن بواسطة خوارزمية سرب الجسيمات والشبكة العصبية الاصطناعية

حسين رحيم جاسم [1]*، احمد ريسان حسين [2]

[1،2] قسم الهندسة الكهربائية، كلية الهندسة، جامعة ميسان، العراق

*البريد الالكتروني: enghs2308@uomisan.edu.iq

المستخلص

تفرض الشبكات المصغرة المعزولة تحديات إدارية صعبة؛ بسبب الحاجة لضمان تقاسم مستقر للطاقة ومرونة ديناميكية في ظل التغيرات السريعة في الحمل. ولا يمكن للمتحكمات التقليدية ذات الكسب الثابت ضمان الأداء الديناميكي المطلوب، كما أنّها تواجه المفاضلة الأساسية بين تنظيم الجهد ودقة تقاسم الطاقة الكامنة في التحكم بالإسقاط القياسي، ونظراً لهذه الفجوة البحثية الهامة، تقترح هذه الورقة استراتيجية تحكم متتالية جديدة تعتمد حلقة خارجية هجينة يتم فيها دمج متحكم التناسب والتكامل والاشتقاق مع آلية الإسقاط .هذا الدمج يسمح بالحصول على ميزة إلغاء أخطاء الحالة المستقرة وتحسين التخميد العابر، بينما تضمن الحلقة الداخلية ثابتة الكسب من نوع التناسب والتكامل فصلاً سريعاً للتيار/الجهد. والأهم من ذلك، يجمع النظام بين المنهجية الهجينة لخوارزمية تحسين سرب الجسيمات والشبكة العصبية الاصطناعية لتحقيق تحسين تكيفي متزامن لجميع معاملات الحلقة الخارجية، وهي معاملات متحكم التناسب والتكامل والاشتقاق الثلاثة ومعاملي الإسقاط الاثنين، وذلك ضمن منهجية من مستويين. وتطبيقياً، يستخدم هذا النهج خوارزمية تحسين سرب الجسيمات للحصول على المكاسب المثلى عالمياً في وضع عدم الاتصال، بينما تقوم الشبكة العصبية الاصطناعية بتعلّم هذا الإسقاط المعقد، مما يحول عملية التحسين المُكلفة حسابياً إلى مشكلة تنبؤ آني للمكاسب في الزمن الحقيقي. وقد تم التحقق من متانة وكفاءة النظام المطور بشكل شامل على عاكسات متماثلة فيزيائياً في ظل نظام تحكم غير متماثل يهدف إلى فرض نسبة تقاسم طاقة صعبة جداً تبلغ ٦٠ 40% %وتؤكد نتائج المحاكاة تفوق المتحكم التكيفي المصمم، حيث تم تحقيق انخفاض كبير في التجاوز وزمن الاستقرار، وتحسن كبير في دقة تقاسم الطاقة، وتقليل أدنى لانحرافات الجهد/التردد والتشوه التوافقي الكلي .تثبت هذه التقنية أنّها حل ممكن وذو موثوقية عالية للتحكم اللامركزي في بيئات الشبكات المصغرة المعزولة والديناميكية.